Observation of a second Dirac point in a graphene/superconductor bilayer

Gopi Nath Daptary,[1,2] Eyal Walach,[1] Udit Khanna,[1] Efrat Shimshoni,[1] and Aviad Frydman[1]
[1]Department of Physics, Jack and Pearl Resnick Institute and the Institute of Nanotechnology and Advanced Materials, Bar-Ilan University, Ramat-Gan 52900, Israel
[2]Department of Physics and Astronomy, National Institute of Technology, Rourkela 769008, India

(Received 18 January 2021; revised 27 May 2024; accepted 12 July 2024; published 1 August 2024)

Two-dimensional (2D) materials have attracted vast research interest since the breakthrough discovery of graphene. One major benefit of such systems is the ability to tune the Fermi level through the charge neutrality point between electron and hole doping. Here we show that single layer graphene coupled to the low-density superconductor indium oxide (InO) exhibits two charge neutrality points, each of them representing electronic regions in which the carrier density can be tuned from hole to electron dominated. This is not seen in clean graphene or in a bilayer where the carrier density is extremely low. We suggest that the second charge neutrality point results from regions in the graphene layer just below superconducting islands in InO, where pairing is induced via the proximity effect; gating of this hybrid system therefore allows the tuning from hole to electron superconductivity through an ultralow carrier density regime. We propose this as a "superconducting Dirac point (SDP)" where intravalley scattering is greatly enhanced. Our results suggest that the electronic states around SDP behave like those in a strongly coupled superconductor.

DOI: 10.1103/PhysRevMaterials.8.084802

I. INTRODUCTION

Over the past few decades, proximity induced superconductivity in 2D materials has been of great interest because of the potential to realize non-Abelian topological excitations [1–4]. The rapid progress in fabrication of van der Waals two-dimensional (2D) materials [5–7] offers a wide variety of platforms that may be used for such studies. However, most of these materials exhibit a finite band gap at the charge neutrality point, and superconductivity emerges only at substantial carrier densities. In this respect, graphene is unique: it exemplifies a true semimetal where ungapped band touchings [Dirac points in single layer graphene (SLG)] at the two valleys are protected by the lattice symmetries, and by the tiny spin-orbit coupling [8]. While graphene does not feature superconductivity in its natural form, coupling it to a superconductor may lead to novel physics. One example is the formation of chiral Andreev edge states (CAESs), a trademark signature of chiral Majorana fermion modes, which have been experimentally observed at the interface of graphene quantum Hall states and superconductors [9]. Several fascinating phenomena such as crossed Andreev conversion (CAC) [10] and inter-Landau level Andreev reflection [11] have been observed at these interfaces.

Proximity superconductors used in most cases in the past were conventional *s*-wave superconducting material with carrier density (n), substantially larger than that of graphene. This is typically accompanied by a heavy doping of the proximitized regions of graphene, shifting their Fermi level far above the Dirac point. In contrary, coupling graphene to a low-density superconductor may generate a situation where the Fermi energy of the proximitized and normal regions of graphene are similar, thus giving rise to interesting phenomena [12]. In this work, we study SLG in which a finite pairing gap has been induced by proximity to a low-density, strongly disordered superconductor. We find that this system exhibits two charge neutrality points. We suggest that one is related to normal graphene and the other related to proximitized superconducting graphene. Such a situation makes it possible to tune the proximitized regions between an electronic Cooper pair to a hole Cooper pair based superconductor, enabling access to regimes where conventional *s*-wave pairing is maintained at very small carrier densities where the Fermi energy E_F may be smaller than the pairing gap Δ. Such a setup can therefore serve as a platform for future studies of strongly coupled superconductivity in a 2D material.

II. EXPERIMENTAL DETAILS

For inducing low-density superconductivity into graphene we use amorphous indium oxide (InO) films as proximity superconductors. InO films, despite being morphologically uniform, have been shown to include emergent granularity in the form of superconducting puddles embedded in an insulating matrix [13]. Experiments have revealed evidence for superconducting vortices and a finite energy gap even in the (globally) insulating phase of InO [14–18], demonstrating that the loss of global phase coherence does not necessarily cause the pairing gap Δ to close, as the decoupled islands still remain superconducting. This phase, in which local electronic pairing is present in an insulating system, has been dubbed a "Bosonic insulator." Hence, the presence of disorder can separate the temperature T^* where pairing develops in the grains with the development of a soft gap in the local density of states, and the resistive T_c, where the superfluid density becomes finite.

The samples in our experiments were 30-nm-thick films of InO that were *e*-beam evaporated on a patterned chemical

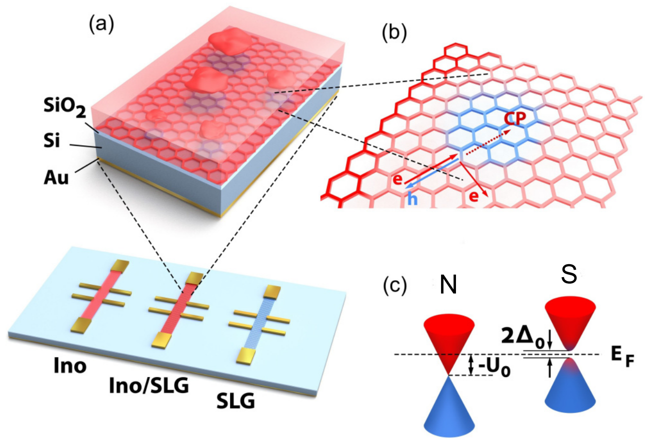

FIG. 1. (a) Schematic diagram of the three devices (bare InO, bilayer of SLG/InO, and bare SLG) grown on a Si/SiO_2 substrate (bottom panel). A gold evaporated electrode on the bottom is used to apply a back-gate voltage on the SLG enabling the tuning of the Fermi energy E_F. A zoom of the SLG/InO (top panel) illustrates superconducting grains within the InO insulating layer. These induce proximity based regions of finite pairing (light blue) in the graphene layer. (b) In the SLG an electron impinging on the NS interface is reflected as a quasiparticle which has electron [(e), red arrow] and hole [(h), blue arrow] components while transferring a Cooper pair (CP) into the superconducting region. (c) Band diagram of normal parts of the SLG/InO (left) and the proximity induced superconducting puddles (right) characterized by a Fermi energy difference U_0 and an induced pairing gap Δ_0, when tuned to the special point $E'_F = E_F + U_0 = 0$ (see text).

vapor deposition grown SLG. For reference, we simultaneously prepared samples of bare SLG and InO [Fig. 1(a)]. The O_2 partial pressure during evaporation (in the range 2–8 $\times 10^{-5}$ Torr) determined the carrier density, of the disordered superconductor in the range 10^{19}–10^{20} cm^{-3} [19], a few orders of magnitude smaller than typical n in metals. This work includes five SLG/InO stacks in which this partial pressure was 8×10^{-5} (S1), 6.2×10^{-5} (S2), 4×10^{-5} (annealed) (S3), 4×10^{-5} (S4), and 2×10^{-5} (S5). As n increases and the sheet resistance R_{sq} decreases, the InO films undergo a superconductor-insulator transition (SIT) tuned by carrier concentration. In this work, all samples of the InO were insulating except for S5 in which the InO was superconducting [Fig. 2(a)].

III. RESULTS AND DISCUSSION

As noted above, insulating InO films contain emergent superconducting islands embedded in an insulating matrix. The small superconducting puddles have a higher electron density than the insulating background. Coupling such a "superconducting insulator" to a SLG film gives rise to a unique situation. We propose that the underlying graphene develops regions with a nonvanishing superconducting gap just below the superconducting islands due to the proximity effect [Fig. 1(a)]. Depending on electrostatic details the electron density in the proximitized puddles may be locally depleted or inflated relative to the normal graphene background. As a consequence, the puddles can be described by two parameters, Δ_0 and U_0, denoting the induced superconducting gap and the potential difference between the puddles and the background, respectively.

Transport measurements (discussed below) show that in our case, U_0 is negative; as a consequence of the low carrier density in the InO film, it is furthermore not much larger than the Fermi energy in the normal graphene regions, E_F. Therefore, the effective Fermi energy in the proximitized regions, $E'_F = E_F + U_0$, is lower than E_F. This provides the experimental opportunity to tune the chemical potential through the charge neutrality points of both the normal and the proximitized (superconducting) regions [see Fig. 1(c)]. In the remainder of this paper, the former is named the Dirac point (DP) and the latter is dubbed the superconducting Dirac point (SDP). The present situation may be contrasted with the case of proximity effect due to metallic superconductors, for which U_0 is typically positive and much larger than E_F, pushing the SDP beyond the regime accessible in experiments. Most of the previous theoretical works have been restricted to the regime of large U_0 as well [20,21]. The presence of two charge neutrality points can be inferred by measuring the bilayer resistance as a function of gate voltage V_g, which controls E_F. Figure 2(b) shows $R_{sq}(V_g)$ for a SLG and a series of SLG/InO bilayers (samples S1–S4). For the bare SLG, the DP occurs at a gate voltage $V_g \approx 50$ V [see Fig. 2(c)] indicating that the graphene is hole doped due to adsorption of atmospheric dopants such as H_2O and O_2 [22]. Covering the SLG by an InO film induces electron doping in the graphene layer so its DP shifts to negative gate voltages. At the same time, an additional resistance peak (identified as the SDP) emerges to the right of the DP, which grows with increasing n of the InO. Hall effect measurements performed on the bilayer samples [Fig. 2(c)] show that the DP is indeed the global point of charge neutrality. However, the SDP also has a very distinct signature on the $R_{xy}(V_g)$ curves and one can envision that it superimposes an additional charge neutrality feature on the overall Dirac behavior background. In our experiments, the DP feature is consistently wider than the SDP, possibly due to the larger and less homogeneous normal regions compared to the SC puddles, which leads to a spread in n and broadening of the Dirac point. Here, we identified the global charge neutrality point observed in Hall measurements with the DP because the area fraction of superconducting puddles in insulating InO films is small, rendering most of the SLG to be in the normal region. The meaning of "global charge neutrality" is different for the case of superconducting InO films, for which the area fractions of proximitized and normal regions are comparable. This case was studied in Ref. [12].

Such a two-DP structure has been observed previously in graphene p-n junctions [23]. We suggest that in our case the second resistance peak is related to superconductivity since the granularity in disordered films such as InO are attributed to superconducting pairing [15,16,24] leading naturally to phase separation of regions of different n. This view is supported by the case where the charge density of InO is higher and Josephson tunneling dominates the physics [12]. Indeed, the two-dip structure is a low temperature feature which gets weaker, and eventually vanishes, with increasing temperature. Figure 2(d) shows the sheet resistance as a function of V_g of sample S3 at different temperatures. While the left peak (the

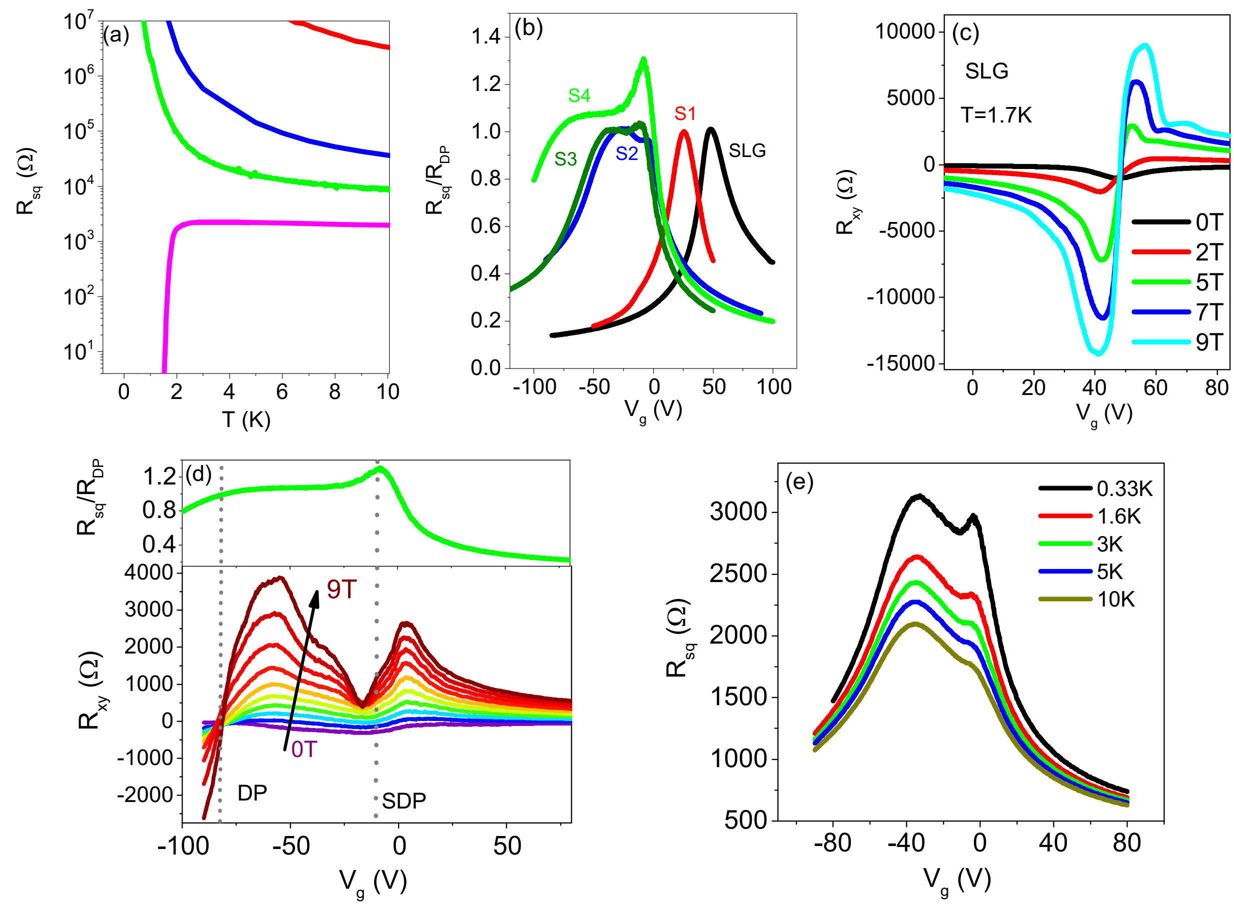

FIG. 2. (a) Sheet resistance R_{sq} of a series of bare InO films as a function of temperature grown at different O_2 pressure, 8×10^{-5}, 6.2×10^{-5}, 4×10^{-5}, and 2×10^{-5} Torr from top to bottom respectively. (b) R_{sq}, normalized by the resistance at the Dirac point (DP), as a function of the gate voltage V_g of a SLG (black solid line) and SLG/InO bilayer S1–S4 from right to left respectively (S5 is superconducting, and hence it shunts the SLG). Measurements were performed at $T = 1.7$ K and $B = 0$ T. (c) Hall resistance R_{xy} as a function of V_g of SLG at $T = 1.7$ K. (d) Lower panel: Hall resistance, R_{xy}, of sample S4 as a function of V_g at $T = 1.7$ K and different magnetic field $B = 0$–9 T (in steps of 1 T). Note that the DP is at $V_d = -80$ V. Upper panel: R_{sq} of sample S4 as a function of V_g at $T = 1.7$ K and $B = 0$ T. (e) R_{sq} of sample S3 as a function of V_g at different temperatures and $B = 0$ T.

DP) is unchanged, the right peak (the SDP) is only observable at $T \sim 10$ K. Interestingly, the SDP persists to temperatures that are higher than the T_c of the superconducting phase of InO. In this respect, we note that STM measurements on a film of InO with (global) $T_c \approx 3$ K have detected a finite (local) Δ up to temperatures of ≈6.5 K [14]. In the insulator, this Δ is predicted to grow further and increase as disorder increases [24]. The real pairing critical temperature, T^*, of the superconducting islands of InO is yet unknown and may be quite large.

The SDP has also a distinct signature on the weak localization (WL) contribution to the conductivity. WL in graphene is very different than that in conventional metals. Because of the presence of two valleys in k space and the chiral nature of the charge carriers, the interference of carriers is not only sensitive to the inelastic scattering rate, but also to certain elastic scattering processes that do not maintain the chirality and cause decoherence. Charge carriers in graphene acquire a Berry phase of π upon completing a closed path, leading to weak antilocalization (WAL) and positive magnetoresistance (MR). However, intravalley chiral-symmetry-breaking scattering, as well as the anisotropy induced by triagonal warping, destroy coherence and thus suppress WAL at an intravalley scattering rate τ_*^{-1} [25]. On the other hand, intervalley scattering (at rate τ_i^{-1}) can protect chirality and also nullify the effect of the Berry phase leading to WL and negative MR. Hence, the interplay of the intra- and intervalley scattering processes determine the amplitude and sign of the MR [26].

At low magnetic field, the MR $[\delta R_{sq}(B) = R_{sq}(B) - R_{sq}(0)]$ can be analyzed using the following expression from [27], which depends on several field scales (inelastic B_ϕ and elastic B_i, B_*) of the system:

$$\delta R_{sq}(B) = \frac{-e^2 R_{sq}^2(0)}{\pi h}\left[F\left(\frac{B}{B_\phi}\right) - F\left(\frac{B}{B_\phi + 2B_i}\right) - 2F\left(\frac{B}{B_\phi + B_*}\right)\right], \tag{1}$$

where $F(z) = \ln(z) + \psi(0.5 + \frac{1}{z})$. Here, ψ is the digamma function. The phase breaking length L_ϕ and elastic intervalley (intravalley) scattering lengths L_i (L_*) can be defined as $L_{\phi,i,*} = \sqrt{\frac{\hbar}{4eB_{\phi,i,*}}}$.

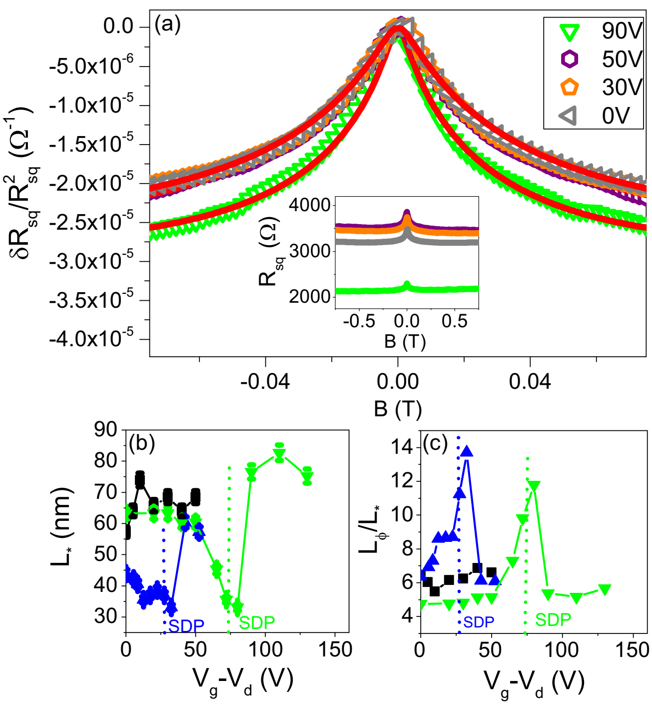

FIG. 3. (a) Relative sheet resistance, $\delta R_{sq}/R_{sq}^2$ versus magnetic field as a function of $V_g - V_d$ of sample S4 including fits to Eq. (1). Raw data of these curves is shown in the inset. (b) L_* and (c) L_ϕ/L_* extracted from these fits as a function of $V_g - V_d$ for SLG (black), S2 (blue), and S4 (green). Measurements were performed at $T = 1.7$ K. The error in L_* isaround 3%, calculated by analysis of the best fits of Eq. (1).

Figure 3(a) shows the resistance as a function of the magnetic field of sample S4 at different values of V_g and $T = 1.7$ K, exhibiting WL in the low field regime. From these curves we extract the values of the three length scales, L_ϕ, L_i, and L_* defined above. L_* as a function of V_g [Fig. 3(b)] reveals a clear minimum at the SDP, implying that *elastic intravalley* scattering is greatly enhanced at this point. In contrast, L_i is relatively constant irrespective of the InO details or V_g. L_ϕ/L_*, which determines the magnitude of the WL [26], peaks at the SDP [Fig. 3(c)].

IV. THEORETICAL MODEL

To further substantiate the presence of superconducting regions in graphene, we theoretically analyze how these proximitized islands, which present an additional source of scattering, affect the transport properties of our bilayers. Specifically we consider the role of *elastic* scattering processes occurring at the interface of normal (N) and proximitized (S) regions of graphene [Fig. 1(b)]. Processes involving coherent scattering from multiple puddles are ignored here. This is justified in our case, as the superconducting puddles are relatively isolated, representing a small fraction of the total area.

NS junctions have been studied previously in both normal metals [28] and graphene [20], and may lead to either normal or Andreev reflection if the energy (ϵ) of the incoming electron is less than or comparable to Δ_0. In graphene, depending on the ratio of ϵ and E_F, the Andreev process may be retro (for $\epsilon \ll E_F$), in which the reflected hole retraces the original electron's path, or specular ($\epsilon \gg E_F$). Earlier studies of graphene NS junctions [20] were mostly limited to the case of metallic superconductors, for which the potential difference U_0 between N and S is large and positive. In light of our experimental observations, we reanalyze this setup for the case of U_0 negative and comparable to E_F. In particular, we will focus on the regime close to the SDP ($|U_0| \sim E_F$) which is defined as the charge neutrality point of the S.

Andreev reflection is necessarily an intervalley scattering process in graphene due to the time-reversal invariant pairing potential. On the other hand, the normal reflection is expected to be dominantly an intravalley process as the NS junction is expected to be smooth at the scale of the lattice. Thus, for brevity, we consider the Hamiltonian (given below) which acts on states involving electrons from a given valley and spin polarization, and holes from the other valley and opposite spin polarization. For a planar NS junction (parallel to, say, the y direction), the general Hamiltonian may be written as

$$H = \begin{pmatrix} H_0 - E_F(x) & \Delta(x)e^{i\phi} \\ \Delta(x)e^{-i\phi} & E_F(x) - H_0 \end{pmatrix}, \tag{2}$$

where $H_0 = -i(\sigma_x\partial_x + \sigma_y\partial_y)$, $\hbar v_F = 1$, and σ represents the sublattice degree of freedom. The $x < 0$ half-plane is assumed to be in the normal region with $\Delta(x<0) = 0$ and $E_F(x) = E_F$, while the $x > 0$ region is assumed to be superconducting with $\Delta(x>0) = \Delta_0$ and $E_F(x>0) = E'_F = E_F + U_0$. Assuming the incoming state from N is a right-moving electron, the general state in the N region may be written as

$$\Psi_N(\epsilon, q) = \psi_{e,R} + r_{ee}\psi_{e,L} + r_{eh}\psi_{h,R}. \tag{3}$$

Here, r_{ee} and r_{eh} are the amplitudes of an electron scattering from the S as an electron and hole respectively. The wave functions $\psi_{e/h,R/L}$ were presented in Ref. [20]. For $\epsilon < \Delta_0$, there are only two physical solutions (for each energy and transverse wave vector q) which exponentially decay deep inside the superconducting region. These may be written as

$$\psi_+ = e^{i(k_x x + qy) - \kappa x} \begin{pmatrix} e^{i\beta\times\mathrm{sign}(E'_F)} \\ d_+ e^{i\beta\times\mathrm{sign}(E'_F)} \\ e^{-i\phi} \\ d_+ e^{-i\phi} \end{pmatrix}, \tag{4}$$

$$\psi_- = e^{i(-k_x x + qy) - \kappa x} \begin{pmatrix} e^{-i\beta\times\mathrm{sign}(E'_F)} \\ d_- e^{-i\beta\times\mathrm{sign}(E'_F)} \\ e^{-i\phi} \\ d_- e^{-i\phi} \end{pmatrix}. \tag{5}$$

Here $\cos\beta = \epsilon/\Delta_0$, $k_x = |\mathrm{Re}[p_x]|$, $\kappa = |\mathrm{Im}[p_x]|$, where

$$\sqrt{p_x^2 + q^2} = |E'_F| \pm i\sqrt{\Delta_0^2 - \epsilon^2}, \quad \text{and} \tag{6}$$

$$d_\pm = \frac{E'_F \pm i\,\mathrm{sgn}(E'_F)\sqrt{\Delta_0^2 - \epsilon^2}}{\pm k_x + i\kappa - iq}. \tag{7}$$

Thus, the most general wave function (given ϵ and q) in the two superconducting regions is

$$\Psi_S(\epsilon, q) = c_+\psi_+ + c_-\psi_-. \tag{8}$$

We note that the wave functions $\psi_\pm$ in (4) and (5) are completely general and hold for any value of E'_F. These reduce to

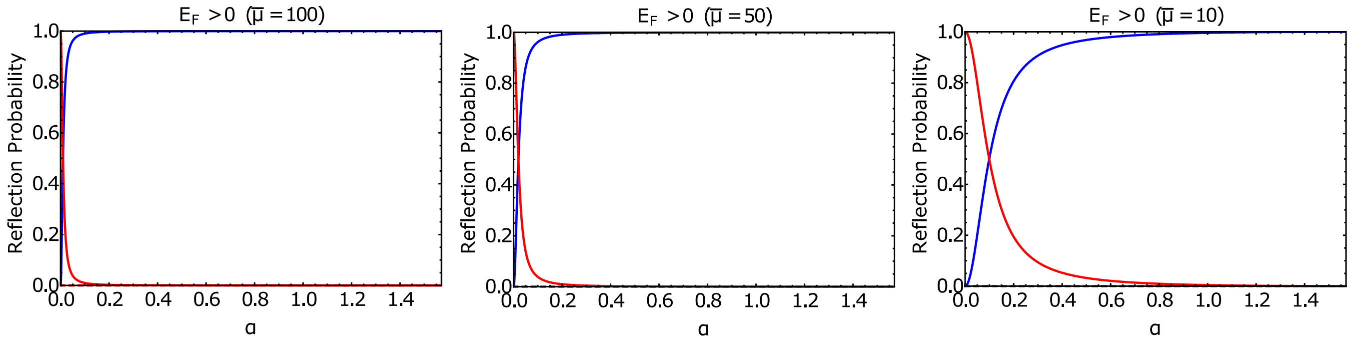

FIG. 4. Reflection probabilities (Andreev in red, normal in blue) vs angle of incidence α for different $\bar{\mu} = |E_F|/\Delta_0$ close to the SDP. Here we assumed electron doping in the normal region ($E_F > 0$). The left, center, and right panels correspond to $\bar{\mu} = 100, 50, 10$ respectively.

the wave functions employed in Ref. [20] in the limit of large doping in the SC ($U_0 \gg E_F$).

The reflection coefficients may be evaluated for any value of the parameters by imposing continuity on the wave function across the NS junction, i.e., $\Psi_N(\epsilon, q)|_{x=0} = \Psi_S(\epsilon, q)|_{x=0}$. Here we shall focus on the behavior of the scattering amplitudes (r_{ee} and r_{eh}) at low energies close to the SDP ($U_0 \sim -E_F$). Specifically, we shall assume $|E'_F| \ll \sqrt{(\Delta_0^2 \sin^2\beta + q^2)}$ which is valid around the SDP ($|E'_F| \ll \Delta_0$) for all q if the energies are sufficiently small energy, $\epsilon \ll \Delta_0$ (or $\beta \sim \pi/2$). In this case we find (to leading order)

$$d_\pm \approx \pm \mathrm{sgn}(E'_F) \times e^\Gamma, \quad \text{where} \tag{9}$$

$$\sinh(\Gamma) = \frac{q}{\Delta_0 \sin\beta}. \tag{10}$$

The leading order reflection amplitudes turn out to be

$$r_{ee} = \frac{e^\Gamma e^{-i(\alpha_e+\alpha_h)} - e^{-\Gamma}}{e^\Gamma e^{i(\alpha_e-\alpha_h)} + e^{-\Gamma}}, \tag{11}$$

$$r_{eh} = -2i\frac{\sqrt{\cos(\alpha_e)\cos(\alpha_h)}}{e^\Gamma e^{i(\alpha_e-\alpha_h)} + e^{-\Gamma}}. \tag{12}$$

These satisfy $|r_{ee}|^2 + |r_{eh}|^2 = 1$ due to conservation of probability current. Here, $\alpha_{e/h}$ are the angles of incidence/reflection for the electron and hole, defined as

$$\alpha_e = \sin^{-1}\left[\frac{q}{|E_F + \epsilon|}\right], \quad \alpha_h = \sin^{-1}\left[\frac{q}{|E_F - \epsilon|}\right]. \tag{13}$$

Since we are only interested in energies much smaller than the gap, we approximated β by $\pi/2$ in (11) and (12) in order to simplify the expressions. Therefore, $\Gamma = \frac{q}{\Delta_0} \approx \bar{\mu}\sin(\alpha_e)$ in (11) and (12), where $\bar{\mu} = \frac{|E_F|}{\Delta_0}$. We note that the amplitudes are independent of E'_F. This is similar to what happens in the limit of large doping $|E'_F| \gg \Delta_0$ [20]. However, we have not made any assumptions about E_F and Δ_0. In light of our observations, we further assume that the SDP and DP are not too close in energy, i.e., $|E'_F - E_F| \gg \Delta_0 \gg \epsilon$ (which is equivalent to $\bar{\mu} \gg 1$). Then $\alpha_e \approx \alpha_h \equiv \alpha$ defined by $|E_F|\sin(\alpha) = q$, and the amplitudes simplify to

$$r_{ee} = e^{-i\alpha}[\cos(\alpha)\tanh(\bar{\mu}\sin(\alpha)) - i\sin(\alpha)], \tag{14}$$

$$r_{eh} = -i\frac{\cos(\alpha)}{\cosh(\bar{\mu}\sin(\alpha))}. \tag{15}$$

Notably, $|r_{ee}| = 0$ and $|r_{eh}| = 1$ at normal incidence ($\alpha = 0$), while $|r_{ee}| \approx 1$ and $|r_{eh}| \approx 0$ when $\alpha \sim \pi/2$. This change occurs around $\Gamma = 1$, i.e., $\alpha \sim \sin^{-1}\bar{\mu}^{-1} = \sin^{-1}(\frac{\Delta_0}{|E_F|})$. For large $\bar{\mu}$, this switching angle becomes very small, and hence we expect the (intravalley) normal reflections to dominate the (intervalley) Andreev reflections for almost all angles of incidence (close to the SDP). Figure 4 presents the variation of the (low energy) reflection probabilities at the SDP (blue lines: $|r_{ee}|^2$; red lines: $|r_{eh}|^2$), evaluated numerically without any approximations, with the angle of incidence (α) for different values of $\bar{\mu}$. Clearly, the full solution behaves as expected from the approximate answer in (14) and (15) as long as the SDP and DP are sufficiently far away.

We may further use the scattering amplitudes to find the conductance of the NS junction as [20,28]

$$g_{NS} = g_0 \int_0^{\pi/2} d\alpha\, \cos\alpha(1 - |r_{ee}|^2 + |r_{eh}|^2), \tag{16}$$

where g_0 is the conductance of normal graphene (in absence of any scattering). Figure 5 shows how g_{NS} varies with E_F (which may be tuned through the back gate V_g). Clearly, the conductance is minimal at the DP as well as the SDP, and is qualitatively in accordance with the double peak structure of R_{sq} observed in experiments (Fig. 2). DP refers to the charge neutral point of normal graphene ($E_F = 0$), around which the

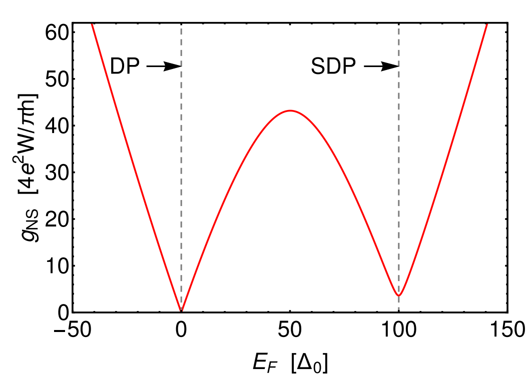

FIG. 5. Conductance of a single NS junction with $U_0 = -100\Delta_0$. The conductance drops to zero at the DP due to the vanishing density of states, and has a pronounced minimum at the SDP due to dominance of normal reflection over Andreev reflection. Here W is the width of the junction in units of $\xi = \hbar v_F/\Delta_0$.

density of states is very small. Thus $g_{\rm NS}(E_{\rm F}=0)=0$ due to vanishing of g_0 despite the normalized conductance, the integral in (16), remaining finite (with a value ~4/3 for this idealized setup) [20].

At the SDP, $E_{\rm F}=-U_0$, or $E'_{\rm F}=0$, the superconducting regions are at the charge neutrality point. Due to the finite pairing amplitude Δ_0 and the low carrier density, the electronic states around the SDP ($|E'_{\rm F}|<\Delta_0$) effectively behave like those in a strongly coupled superconductor. Our analysis of the NS junction in this regime finds that the scattering is dominated by (intravalley) regular reflections. Specifically, $r_{ee}\approx 1$ for almost all angles α, except very close to normal incidence for which $r_{eh}\approx 1$ instead (Fig. 4). This leads to a sharp drop in both $g_{\rm NS}$ as well as the normalized conductance at the SDP. Clearly, this suppression of conductance is only relevant for very low temperatures so that the quasiparticle excitations in S (above the gap) remain inactive. With increasing temperature a new scattering channel, namely transmission into S as a quasiparticle, opens up and gradually becomes more dominant than the reflections. Simultaneously, thermal fluctuations tend to suppress the induced superconductivity itself. Together these two effects act to restore the conductance at the SDP to a finite value. Thus, the behavior of $g_{\rm NS}$ at the SDP is consistent with our observation of a sharp low-temperature peak in the resistance [Fig. 2(b)] which gradually decreases with increasing temperature. We further note that the dominance of (intravalley) normal reflections around the SDP (at low temperatures) is also consistent with a minimum in the elastic intravalley scattering length L_* [Fig. 3(b)] around this peak. Hence, our analysis of the NS junction strongly supports the identification of this low-temperature feature with the SDP.

V. CONCLUSION

In summary, we suggest that graphene proximitized by a low density superconductor can effectively access the ultralow carrier density regime as it is tuned from hole to electron superconductivity via a charge neutrality point. In this regime one may potentially realize the strongly coupled superconductor limit in which the superconducting gap is of the order of the Fermi energy. For our SLG/InO bilayers, in the gating range between the DP and SDP, the S regions are hole doped while the N regions are electron doped. The opposite polarity of the two regions leads to a regime with a distinct phenomenology [12]. Our work motivates further investigation of various aspects of superconductivity in this regime. This includes its potential utility for supporting localized as well as chiral Majorana modes [9], and as a platform for performing quantum computations [29]. Moreover, the quantum Hall regime, at high magnetic fields, may support chiral Andreev edge states. A study of our bilayers at high magnetic fields, potentially exhibiting such states, is currently being performed.

ACKNOWLEDGMENTS

We are grateful for technical help from A. Roy and I. Volotsenko and for illuminating discussions with N. Trivedi and J. Ruhman. G.N.D. and A.F. were supported by the Israel National Fund, ISF Grant No. 1499/21. E.W., U.K., and E.S. were supported by US-Israel Binational Science Foundation (BSF) Grant No. 2016130, NSF-BSF Grant No. 2018726, and Israel Science Foundation (ISF) Grant No. 993/19. U.K. was also partially supported by the Resnick fellowship.

[1] L. Fu and C. L. Kane, Phys. Rev. Lett. **100**, 096407 (2008).

[2] Y. Oreg, G. Refael, and F. von Oppen, Phys. Rev. Lett. **105**, 177002 (2010).

[3] R. S. K. Mong, D. J. Clarke, J. Alicea, N. H. Lindner, P. Fendley, C. Nayak, Y. Oreg, A. Stern, E. Berg, K. Shtengel, and M. P. A. Fisher, Phys. Rev. X **4**, 011036 (2014).

[4] D. J. Clarke, J. Alicea, and K. Shtengel, Nat. Phys. **10**, 877 (2014).

[5] K. Novoselov, A. Mishchenko, A. Carvalho, and A. H. C. Neto, Science **353** (2016).

[6] P. Ajayan, P. Kim, and K. Banerjee, Phys. Today **69**(9), 38 (2016).

[7] D. L. Duong, S. J. Yun, and Y. H. Lee, ACS Nano **11**, 11803 (2017).

[8] A. H. Castro Neto, F. Guinea, N. M. R. Peres, K. S. Novoselov, and A. K. Geim, Rev. Mod. Phys. **81**, 109 (2009).

[9] L. Zhao, E. G. Arnault, A. Bondarev, A. Seredinski, T. F. Larson, A. W. Draelos, H. Li, K. Watanabe, T. Taniguchi, F. Amet *et al.*, Nat. Phys. **16**, 862 (2020).

[10] G.-H. Lee, K.-F. Huang, D. K. Efetov, D. S. Wei, S. Hart, T. Taniguchi, K. Watanabe, A. Yacoby, and P. Kim, Nat. Phys. **13**, 693 (2017).

[11] M. R. Sahu, X. Liu, A. K. Paul, S. Das, P. Raychaudhuri, J. K. Jain, and A. Das, Phys. Rev. Lett. **121**, 086809 (2018).

[12] G. N. Daptary, U. Khanna, E. Walach, A. Roy, E. Shimshoni, and A. Frydman, Phys. Rev. B **105**, L100507 (2022).

[13] D. Kowal and Z. Ovadyahu, Solid State Commun. **90**, 783 (1994).

[14] B. Sacépé, T. Dubouchet, C. Chapelier, M. Sanquer, M. Ovadia, D. Shahar, M. Feigel'Man, and L. Ioffe, Nat. Phys. **7**, 239 (2011).

[15] S. Poran, E. Shimshoni, and A. Frydman, Phys. Rev. B **84**, 014529 (2011).

[16] D. Sherman, G. Kopnov, D. Shahar, and A. Frydman, Phys. Rev. Lett. **108**, 177006 (2012).

[17] G. Kopnov, O. Cohen, M. Ovadia, K. H. Lee, C. C. Wong, and D. Shahar, Phys. Rev. Lett. **109**, 167002 (2012).

[18] A. Roy, E. Shimshoni, and A. Frydman, Phys. Rev. Lett. **121**, 047003 (2018).

[19] Z. Ovadyahu, J. Phys. C **19**, 5187 (1986).

[20] C. W. J. Beenakker, Phys. Rev. Lett. **97**, 067007 (2006).

[21] D. K. Efetov, L. Wang, C. Handschin, K. Efetov, J. Shuang, R. Cava, T. Taniguchi, K. Watanabe, J. Hone, C. Dean *et al.*, Nat. Phys. **12**, 328 (2016).

[22] Y. J. Shin, Y. Wang, H. Huang, G. Kalon, A. T. S. Wee, Z. Shen, C. S. Bhatia, and H. Yang, Langmuir **26**, 3798 (2010).

[23] N. Stander, B. Huard, and D. Goldhaber-Gordon, Phys. Rev. Lett. **102**, 026807 (2009).

[24] K. Bouadim, Y. L. Loh, M. Randeria, and N. Trivedi, Nat. Phys. **7**, 884 (2011).
[25] F. V. Tikhonenko, D. W. Horsell, R. V. Gorbachev, and A. K. Savchenko, Phys. Rev. Lett. **100**, 056802 (2008).
[26] F. V. Tikhonenko, A. A. Kozikov, A. K. Savchenko, and R. V. Gorbachev, Phys. Rev. Lett. **103**, 226801 (2009).
[27] E. McCann, K. Kechedzhi, V. I. Fal'ko, H. Suzuura, T. Ando, and B. L. Altshuler, Phys. Rev. Lett. **97**, 146805 (2006).
[28] G. E. Blonder, M. Tinkham, and T. M. Klapwijk, Phys. Rev. B **25**, 4515 (1982).
[29] B. Lian, X.-Q. Sun, A. Vaezi, X.-L. Qi, and S.-C. Zhang, Proc. Natl. Acad. Sci. USA **115**, 10938 (2018).